

SPINDLE SPEED SELECTION IN ADDITIVE FRICTION STIR DEPOSITION FOR DESIRED TEMPERATURE

Tony Schmitz
Machine Tool Research Center
University of Tennessee, Knoxville
Knoxville, TN, USA

INTRODUCTION

Additive friction stir deposition (AFSD) is a solid-state additive manufacturing (AM) process that provides an alternative to beam-based AM processes which melt the material locally to obtain the desired near-net shape geometry [1-2]. Important applications for AFSD include part repair and preform production for castings, forgings, spare parts, and parts with short delivery times.

AFSD accomplishes solid-state deposition through plastic deformation of a square cross-section, ductile metal alloy feedstock. A tool-spindle assembly containing a square bore constrains the feedstock as it is fed axially through the spindle and rotated against the build plate or previous layers. Spindle rotation provides heat generation through friction between the deposit and build surface and, subsequently, a reduction in the required flow stress. The feedstock is deposited during movement of the tool at the selected tool feed velocity along the prescribed motion path. The feedstock feed velocity through the tool-spindle is also specified. The combined tool rotation and feed kinematics enable layers to be bonded to the build plate and previous layers to deposit the desired preform geometry; see Fig. 1. The preform is then measured and machined to obtain the final geometry and surface finish [3].

While the advantages of AFSD are well-documented, process parameter selection is currently based on prior experience or trial and error. The research objective for this paper is to provide a physics-based model for AFSD spindle speed selection to achieve a desired deposition temperature. An analytical approach is selected to enable implementation with low computational expense. Deposition temperature is critical because it affects the final mechanical properties. Therefore, an approach to select spindle speed to reach a specific temperature is necessary. This effort is complementary to the numerical simulations reported in the literature [4].

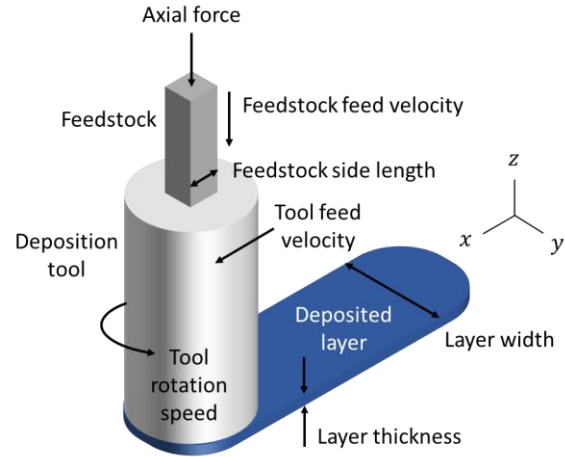


FIGURE 1. AFSD description.

AFSD TEMPERATURE MODEL

In this study, power input to the feedstock (to enable plastic flow and deposition) is related to the material temperature rise, and subsequent flow stress reduction, using Fourier's conduction rate equation. The assumption is that conduction dominates AFSD heat transfer; convection and radiation are neglected in this analysis. Equation 1 provides the relationship between power, P , area under the circular deposition tool, A , thermal conductivity, k , deposition temperature, T , initial temperature, T_0 , and layer thickness, h . Note that the thermal conductivity is temperature-dependent, in general. The deposition geometry is displayed in Fig. 2.

$$\frac{P}{A} = k \frac{(T - T_0)}{h} \quad (1)$$

Power input is provided by two AFSD sources: 1) frictional heating between the rotating deposit and deposition surface; and 2) adiabatic heating due to plastic deformation of the feedstock. The friction power, P_f , is calculated using Eq. 2, where T_f is the torque required to overcome the friction force, F_f , and ω is the tool rotating speed (spindle speed). The torque is rewritten in Eq. 2 as a product of the friction force and radius at which the friction force acts, r_f . Assuming dry sliding

friction, the friction force is rewritten as the product of the normal force in the axial (z) direction, F_z , between the rotating deposit and deposition surface and the Coulomb friction coefficient, μ . Finally, the normal force is replaced by the product of the flow stress, σ , and the deposit area.

$$P_f = T_f \omega = F_f r_f \omega = \mu F_z r_f \omega = \mu \sigma A r_f \omega \quad (2)$$

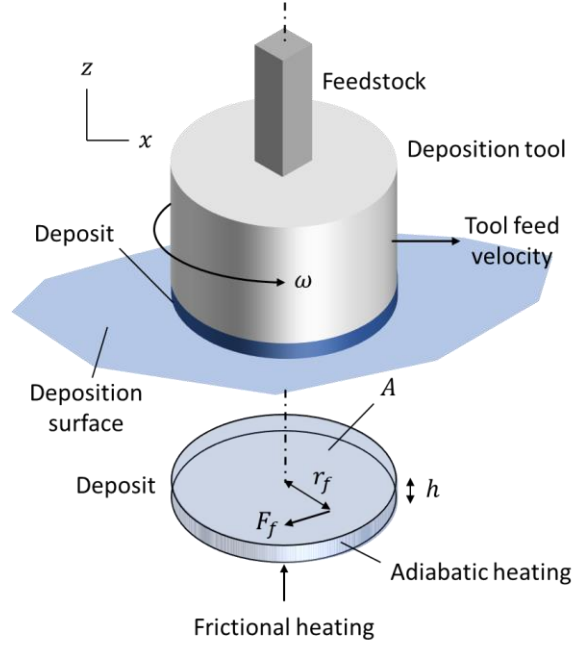


FIGURE 2. AFSD deposition geometry.

The flow stress in Eq. 2 is predicted using the strain, strain rate, and temperature-dependent Johnson-Cook flow stress model provided in Eq. 3, where ϵ is the equivalent plastic strain, $\dot{\epsilon}_e$ is the effective (plastic) strain rate, $\dot{\epsilon}_0$ is the reference strain rate, T_m is the feedstock melting temperature, and A , B , C , n , and m are model parameters obtained from experiments for the selected feedstock material.

$$\sigma = (A + B\epsilon^n) \left(1 + C \ln \frac{\dot{\epsilon}_e}{\dot{\epsilon}_0}\right) \left(1 - \left(\frac{T - T_0}{T_m - T_0}\right)^m\right) \quad (3)$$

The equivalent plastic strain is modeled after forward extrusion in metal forming, where the true strain is calculated using the initial cross-sectional area, A_0 , and extruded cross-sectional area, A_1 . This strain is shown in Eq. 4 for the AFSD geometry, where the initial area is calculated using the square feedstock side length, s , and the extruded area is the perimeter (assumed circular) at the friction radius multiplied by the deposition layer thickness.

$$\epsilon = -\ln \frac{A_0}{A_1} = -\ln \frac{s^2}{2\pi r_f h} \quad (4)$$

The effective strain rate for Eq. 3 is calculated using the kinematics of the rotating-translating deposition tool motion, the gradient of velocity, L , the strain rate tensor, E , and the strain rate, $\dot{\epsilon}$. The tool feed velocity, f , occurs in the x direction and the rotation direction is counterclockwise for the deposition tool; see Fig. 3, where the u and v velocity components are also shown. The associated displacement and velocity expressions are given in Eqs. 5-8, where ϕ is the time-dependent tool rotation angle.

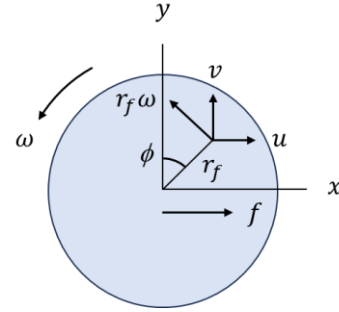


FIGURE 3. Rotating-translating deposition tool kinematics. Spindle rotation is counter-clockwise and tool feed velocity is to the right.

$$x(t) = r_f \sin \phi + ft \quad (5)$$

$$y(t) = r_f \cos \phi \quad (6)$$

$$u(t) = -r_f \omega \cos \phi + f \quad (7)$$

$$v(t) = r_f \omega \sin \phi \quad (8)$$

The two-dimensional gradient of velocity is defined in Eq. 9, where the individual terms in the ratios are calculated by numerical differentiation of Eqs. 5-8. The strain rate tensor is calculated using Eq. 10, where T is the transpose operator.

$$L = \begin{bmatrix} \frac{du}{dx} & \frac{du}{dy} \\ \frac{dv}{dx} & \frac{dv}{dy} \end{bmatrix} \quad (9)$$

$$E = \frac{1}{2}(L + L^T) = \begin{bmatrix} \frac{du}{dx} & \frac{1}{2}\left(\frac{du}{dy} + \frac{dv}{dx}\right) \\ \frac{1}{2}\left(\frac{du}{dy} + \frac{dv}{dx}\right) & \frac{dv}{dy} \end{bmatrix} \quad (10)$$

The strain rate is determined using Eq. 11, where $\langle E, E \rangle$ represents the inner product. Finally, the effective strain rate is calculated using the mean value of Eq. 11 for one tool revolution (i.e., ϕ is varied from 0 to 2π rad in Eqs. 5-8 and the mean value is determined). The adiabatic power, P_a , due to plastic deformation is calculated using Eq. 12, where the Taylor-Quinney coefficient, or ratio

of dissipated heat to plastic work, is taken to be 0.9 for this study.

$$\dot{\varepsilon} = \left(\frac{2}{3} \langle E, E \rangle \right)^{\frac{1}{2}} = \left(\frac{2}{3} (E_{11}^2 + E_{12}^2 + E_{21}^2 + E_{22}^2) \right)^{\frac{1}{2}} \quad (11)$$

$$P_a = 0.9 \sigma \dot{\varepsilon}_e A h \quad (12)$$

Substitution of Eqs. 2 and 12 into Eq. 1 provides a relationship between temperature and spindle speed, where it is noted that the flow stress depends on the effective strain rate and, therefore, the spindle speed.

$$\frac{\mu \sigma A r_f \omega + 0.9 \sigma \dot{\varepsilon}_e A h}{A} = k \frac{(T - T_0)}{h} \quad (13)$$

Solving Eq. 13 for the spindle speed provides an analytical solution for spindle speed selection based on the desired deposition temperature and feedstock material; see Eq. 14. Inputs include the Johnson-Cook flow stress model parameters, temperature-dependent thermal conductivity, layer thickness, tool feed velocity, friction radius, and friction coefficient.

$$\omega = \frac{k(T - T_0) - 0.9 \sigma \dot{\varepsilon}_e h^2}{\mu \sigma r_f h} \quad (14)$$

The relationship between deposition temperature and spindle speed is established using the following steps:

1. select the desired deposition temperature
2. determine the temperature-dependent thermal conductivity from available data
3. calculate the effective strain rate for a pre-selected spindle speed range using the mean value of Eq. 11 for one tool revolution
4. calculate the flow stress over the same spindle speed range from step 3 using Eq. 3
5. evaluate the spindle speed-dependent test function obtained by rewriting Eq. 14, $f(\omega) = k(T - T_0) - 0.9 \sigma \dot{\varepsilon}_e h^2 - \mu \sigma r_f h \omega = 0$, over the same spindle speed range as steps 3 and 4
6. determine the zero crossing for $f(\omega)$ and identify the corresponding spindle speed
7. record the spindle speed for the selected deposition temperature
8. repeat steps 1-7 for the next deposition temperature.

Johnson-Cook flow stress model parameters were obtained from multiple sources, the temperature-dependent thermal conductivity was also found a similar aluminum alloy and is displayed in Fig. 4, the tool feed velocity is 126 mm/min, the layer

thickness is 1.5 mm, the friction radius is 9.525 mm (selected to be half the deposition tool radius of 19.05 mm), the friction coefficient is 0.25 (representative of elevated temperature forming conditions in traditional metalworking), the initial temperature is 25 °C, and the feedstock side length is 9.525 mm.

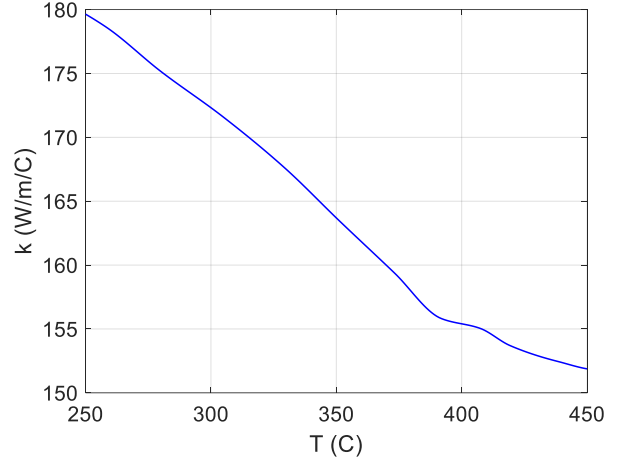


FIGURE 4. Temperature-dependent thermal conductivity for 7075-T651 aluminum.

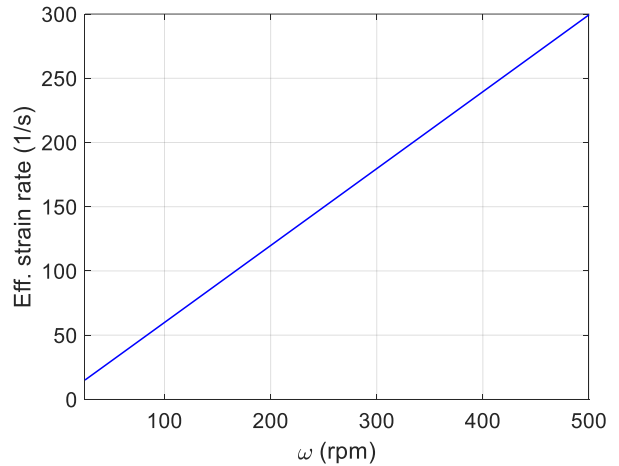


FIGURE 5. Spindle speed-effective strain rate relationship for selected spindle speed range.

The effective strain rate for a spindle speed range of 25 rpm to 500 rpm is displayed in Fig. 5. The corresponding deposition temperature-spindle speed relationships for 11 Johnson-Cook models are shown in Fig. 6. It is observed that the temperature-spindle speed relationships are nonlinear, and the results differ based on the Johnson-Cook model parameters. The mean of all 11 curves from Fig. 6 is displayed in Fig. 7. Results from [5] are also included (red square), where the numerical simulation was performed

using an open-source computational fluid dynamics code. Good agreement is observed.

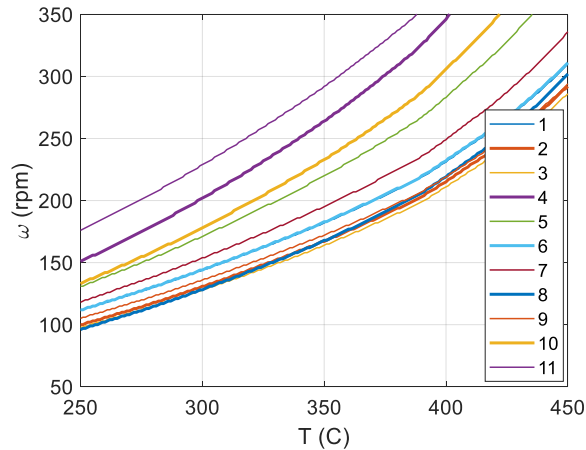


FIGURE 6. Temperature-spindle speed relationships for 11 different 6061 aluminum Johnson-Cook flow stress models for a temperature range of 250 C to 450 C.

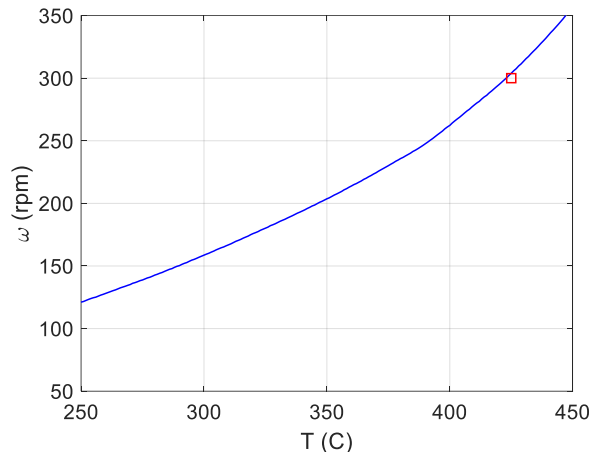


FIGURE 7. Mean deposition temperature-spindle speed relationship from Fig. 6 (blue line) with simulation result (red square) for 6061 aluminum and the same operating parameters [5].

EXPERIMENTAL SETUP

Experiments were completed using a MELD Manufacturing L3 machine; see Fig. 8. The L3 is a three-axis computer numerical control (CNC) machine tool with the deposition head mounted to the vertical (z) axis. The AFSD head includes an actuator and pushrod to provide the downward (normal direction) force. The L3 deposits material in discrete sections, where feedstock is loaded into the pushrod-spindle-tool assembly through the tool opening near the table, where the build plate is mounted. After insertion, the 12.7 mm square by 508 mm long feedstock is forced

downward through the rotating spindle and tool. The feedstock was 7075 aluminum for this study due to its relevance in aerospace applications.

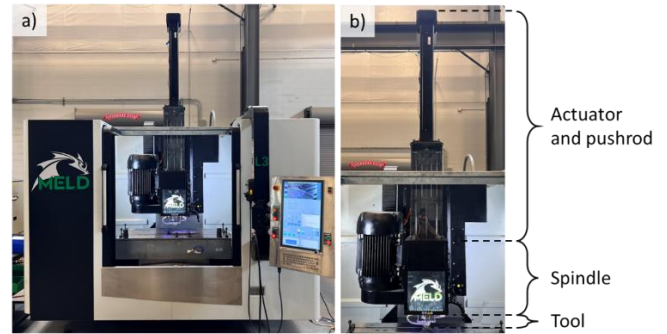


FIGURE 8. a) MELD Manufacturing L3 AFSD machine. b) Details for actuator and pushrod, spindle, and tool assembly.

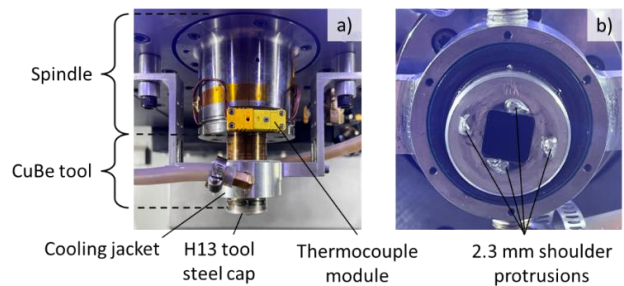


FIGURE 9. a) CuBe tool with H13 tool steel cap, thermocouple connection, and cooling jacket. b) Bottom view of tool showing shoulder face protrusions and 12.7 mm square feedstock bore.

The tool can have a flat shoulder face or can contain features to modify the deposition process similar to friction stir welding tool geometries. For this study, the 38.1 mm diameter, copper beryllium (CuBe) tool from MELD Manufacturing included a 12.7 mm square bore and an H13 tool steel cap with four 2.3 mm tall teardrop-shaped protrusions located at varying radii from the tool center. The tool also had an embedded K-type thermocouple. It was radially offset from the tool center (outside the square bore) and was located axially 0.25 mm to 0.38 mm from the tool face. The thermocouple was used to measure tool temperature with a sampling frequency of 1 Hz. A module was attached to the rotating spindle which transmitted temperature to the machine controller. This temperature was recorded and could be used for closed-loop control, where the spindle speed is adjusted continuously to maintain a commanded temperature. The closed-loop temperature control is enabled and disabled using appropriate m-codes within the part program. It was disabled for this testing since the

intent was to identify the relationship between deposition temperature and a fixed spindle speed. The setup is displayed in Fig. 9, where the external tool cooling jacket is also shown.

RESULTS

Tests were completed to deposit 7075 aluminum feedstock on a 7075-T651 aluminum build plate at selected spindle speeds. Prior to deposition, the build plate surface was roughened using fine grit sandpaper and cleaned with isopropyl alcohol. The temperature was measured using the tool thermocouple to compare with model predictions. A single wall build strategy was selected where each layer was deposited on the previous layer. Each layer included a deposition initiation cycle, which was followed by constant parameter deposition. The deposition initiation cycle was implemented to repeatedly reach an increased temperature which permitted the desired plastic flow. It was automated as a subroutine within the part program.

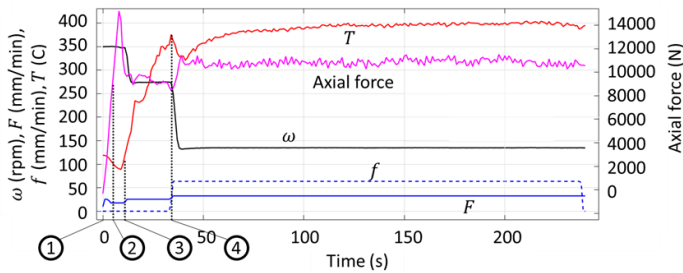


FIGURE 10. Process signals during first layer deposition. Key times in the first layer deposition initiation cycle are identified: 1) set $\omega = 350$ rpm and $F = 25.4$ mm/min and wait for axial force threshold; 2) axial force of 4003 N reached, reduce F to 17.5 mm/min and wait for threshold temperature; 3) temperature threshold of 115 C reached, reduce ω to 275 rpm and increase F to 28 mm/min, hold until final temperature threshold is reached; and 4) final temperature threshold of 370 C reached, command desired constant spindle speed, feedstock feed velocity, and tool feed velocity.

The deposition initiation cycle for the first layer began with the tool located 1.5 mm above the build surface and a spindle speed of $\omega = 350$ rpm at the desired starting point. The feedstock feed velocity was set to $F = 25.4$ mm/min (time 1 in Fig. 10). These parameters were maintained until the threshold axial force of 4003 N (900 lbf) was reached (time 2); this force was measured using the actuator drive current. The feedstock feed

velocity was then reduced to 17.5 mm/min to prevent pushrod overloading until the tool thermocouple temperature threshold of $T = 115$ C was reached (time 3). The spindle speed was reduced to 275 rpm to prevent temperature overshoot at the start of the tool feed across the build plate (or prior layer) surface. The feedstock feed velocity was increased to 28 mm/min to fill the gap between tool and build surface with plastically deformed feedstock. These operating parameters were maintained until the tool temperature reached a final threshold of 370 C (time 4). At this point, the desired constant spindle speed, feedstock feed velocity, and tool feed velocity to be used for deposition were commanded. Note that the feedstock feed velocity values were reduced by 50% in the first layer to ensure successful bonding with the build plate. In all other layers, the feed velocity values listed here were doubled.

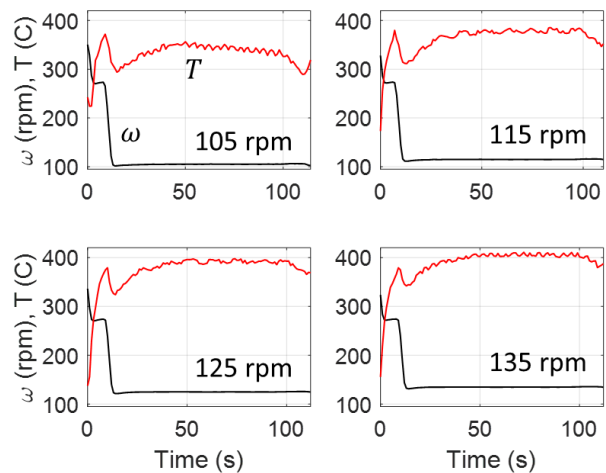


FIGURE 12. Second layer spindle speed and temperature data for four test cases, where $\omega = \{105, 115, 125, \text{ and } 135\}$ rpm. The initial variation in spindle speed (and corresponding temperature response) is due to the deposition initiation cycle.

Four 30-layer walls were deposited using the following parameters: 1.5 mm layer height, $f = 127$ mm/min, $F = 65$ mm/min, and $\omega = \{105, 115, 125, \text{ and } 135\}$ rpm. The corresponding F/f ratio was 0.51 and the approximate layer width was 54.1 mm. The lower and upper spindle speed limits were selected to avoid exceeding the machine's axial force and spindle torque limits, while keeping the temperature below the 7075 aluminum solidus of approximately 477 C to avoid incipient melting. For comparison to model predictions, the mean steady-state temperature from the second layer was selected because, as

noted, each first layer was deposited at 50% of the commanded feedstock and tool feed velocities for the other layers to enable successful bonding to the build plate. The time-dependent spindle speed (due to the deposition initiation cycle) and corresponding temperature are displayed in Fig. 12 for the four spindle speeds. It is observed that the steady-state deposition temperature increases with the selected (constant) spindle speed, as expected.

The AFSD temperature model was used to predict the relationship between deposition temperature and spindle speed for 7075 aluminum. The Johnson-Cook model parameters from seven references (nine total models) were applied. The temperature-dependent thermal conductivity for 7075 aluminum was again used; see Fig. 4. The friction radius was 13.525 mm (half the deposition radius of 27.05 mm), the friction coefficient was 0.25, the initial temperature was 25 C, and the square feedstock side length was 12.7 mm. The deposition temperature-spindle speed relationship from the nine Johnson-Cook models were calculated.

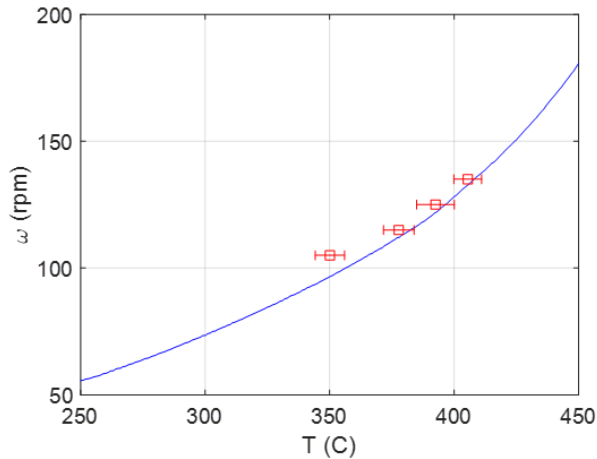


FIGURE 13. Mean deposition temperature-spindle speed relationship (blue line) with experimental results (red squares) at $\omega = \{105, 115, 125, \text{ and } 135\}$ rpm for 7075 aluminum. The error bars indicate 95% confidence intervals.

The mean of the nine curves was used to compare with the four experimental temperature-spindle speed combinations. This comparison between the mean predicted deposition temperature-spindle speed relationship (blue line) and measured tool temperatures for four spindle speeds (red squares) is displayed in Fig. 13. The execution time for Fig. 13 was 2.225 s (Intel Core i7-8850H CPU, 2.60GHz, 32 GB RAM,

Matlab 2023b). The temperature was obtained from the steady-state portions of the four panels in Fig. 12 (50 s to 70 s). The error bars indicate the 95% confidence intervals (i.e., the standard deviation of the steady-state portion was calculated and the error bars were plotted for \pm two times the standard deviation). Good agreement is observed with overlap of the error bars and prediction in three of four cases.

CONCLUSIONS

This paper described a physics-based, analytical model for additive friction stir deposition (AFSD) spindle speed selection to achieve a desired deposition temperature. In the model, power input to the feedstock, which enables plastic flow and deposition, was related to the material temperature rise and subsequent flow stress reduction using Fourier's conduction rate equation. Power input was modeled as frictional heating at the deposit-surface interface and adiabatic heating due to plastic deformation. The flow stress was predicted using the strain, strain rate, and temperature-dependent Johnson-Cook constitutive model for the selected feedstock alloy. Model predictions were compared to AFSD numerical simulation results available in the literature and experiments for aluminum alloys.

ACKNOWLEDGEMENTS

Support for this research was provided by DEVCOM Army Research Laboratory under grant no. W911NF2120020 NSF Engineering Research Center for Hybrid Autonomous Manufacturing Moving from Evolution to Revolution (ERC-HAMMER) under Award Number EEC-2133630.

REFERENCES

- [1] Hang, Z.Y., Jones, M.E., Brady, G.W., Griffiths, R.J., Garcia, D., Rauch, H.A., Cox, C.D. and Hardwick, N., 2018. Non-beam-based metal additive manufacturing enabled by additive friction stir deposition. *Scripta Materialia*, 153, pp.122-130.
- [2] Yu, H.Z. and Mishra, R.S., 2021. Additive friction stir deposition: a deformation processing route to metal additive manufacturing. *Materials Research Letters*, 9(2), pp.71-83.
- [3] Kincaid, J., Charles, E., Garcia, R., Dvorak, J., No, T., Smith, S. and Schmitz, T., 2023. Process planning for hybrid manufacturing using additive friction stir deposition. *Manufacturing Letters*, 37, pp.26-31.
- [4] Kincaid, K.C., MacPhee, D.W., Stubblefield, G.G., Jordan, J.B., Rushing, T.W. and Allison, P.G., 2023. A finite volume framework for the simulation of additive friction stir deposition. *Journal of Engineering Materials and Technology*, 145(3), p.031002.